Biochemical and Biophysical Research Communications 449 (2014) 425–431

Contents lists available at ScienceDirect

Biochemical and Biophysical Research Communications

journal homepage: www.elsevier.com/locate/ybbrc

Structural characterization and interaction of periostin and bone morphogenetic protein for regulation of collagen cross-linking

Eun Young Hwang [a,1], Mi Suk Jeong [a,1], Eun-Kyeong Park [a,1], Jae Ho Kim [b], Se Bok Jang [a,*]

[a] Department of Molecular Biology, College of Natural Sciences, Pusan National University, Jangjeon-dong, Geumjeong-gu, Busan 609-735, Republic of Korea
[b] Department of Physiology, College of Medicine, Pusan National University, Busan 602-735, Republic of Korea

ARTICLE INFO

Article history:
Received 8 May 2014
Available online 22 May 2014

Keywords:
Periostin
Bone morphogenetic protein
Fas1 domains
Molecular interaction

ABSTRACT

Periostin appears to be a unique extracellular protein secreted by fibroblasts that is upregulated following injury to the heart or changes in the environment. Periostin has the ability to associate with other critical extracellular matrix (ECM) regulators such as TGF-β, tenascin, and fibronectin, and is a critical regulator of fibrosis that functions by altering the deposition and attachment of collagen. Periostin is known to be highly expressed in carcinoma cells, but not in normal breast tissues. The protein has a structural similarity to insect fasciclin-1 (Fas 1) and can be induced by transforming growth factor-β (TGF-β) and bone morphogenetic protein (BMP)-2. To investigate the molecular interaction of periostin and bone morphogenetic protein, we modeled these three-dimensional structures and their binding sites. We demonstrated direct interaction between periostin and BMP1/2 *in vitro* using several biochemical and biophysical assays. We found that the structures of the first, second, and fourth Fas1 domains in periostin are similar to that of the fourth Fas 1 domain of TGFBIp. However, the structure of the third Fas 1 domain in periostin is different from those of the first, second, and fourth Fas1 domains, while it is similar to the NMR structure of Fasciclin-like protein from *Rhodobacter sphaeroides*. These results will useful in further functional analysis of the interaction of periostin and bone morphogenetic protein.

1. Introduction

Periostin, which was originally known as osteoblast-specific factor 2, is a secretory protein expressed in collagen-rich fibrous connective tissues, such as periodontal ligament, the aorta, and heart valves [1,2]. Overexpression of periostin by adenoviral infection in cardiac valvulogenic tissue increases the overall viscosity, which is a measure of collagen cross-linking [3–6]. Periostin was first identified as a bone-specific protein and has more recently been implicated in heart valve morphogenesis, oncogenesis, and vascular smooth muscle cells [7–10]. Periostin expression was also found to be increased in head and neck squamous cell carcinoma (HNSCC) when compared with normal tissues [11]. This may be associated with the bone metastatic potential of lung cancers and the progression of breast cancer [12,13]. The molecular mechanism of periostin action in collagen cross-linking has investigated, and the results showed that periostin enhances the proteolytic activation of lysyl oxidase (LOX), which is an enzyme responsible for cross-link formation, and that it is caused by interacting with bone morphogenetic protein (BMP)-1 to promote the collagen cross-linking [14].

Bone morphogenetic proteins (BMPs) are cytokines that belong to the multifunctional transforming growth factor-β (TGF-β) superfamily, which controls growth, proliferation and differentiation of many cell types. In particular, BMPs have been found to be able to induce bone and cartilage formation at ectopic sites *in vivo* [15]. BMP-1 was also shown to provide the activity necessary for proteolytic removal of the C-propeptides of procollagens I–III and precursors of the major fibrillar collagens, as well as to be the prototype of a small group of extracellular metalloproteinases that play manifold roles in regulating formation of the extracellular matrix (ECM). Periostin is known to be induced by BMP2 in MC3T3 cells [16], and BMP2 and BMP signaling induce biological processes involved in early AV valvulogenesis; namely, mesenchymal cell migration and expression of periostin, indicating critical roles of BMP signaling in post-EMT AV cushion tissue maturation and differentiation [17].

Recent research suggested that PNDA-3 (Periostin-binding DNA Aptamer-3) selectively bound to the FAS-1 domain of periostin and disrupted the interaction between periostin and its cell surface

* Corresponding author. Fax: +82 51 581 2544.
E-mail address: sbjang@pusan.ac.kr (S.B. Jang).
[1] These authors contributed equally to this article.

http://dx.doi.org/10.1016/j.bbrc.2014.05.055
0006-291X/

receptors, $\alpha_v\beta_3$ and $\alpha_v\beta_5$ integrins [18]. The essential and minimal domain that is required for PNDA-3 binding has been shown to be the third FAS-1 domain, which is critical to integrin binding. To date, no structural information has been reported regarding periostin and its interaction. In this study, we demonstrated direct interactions between periostin and BMP1/2 *in vitro* using several biochemical and biophysical assays. The periostins first Fas1/third Fas1 and their mutants were successfully purified and analyzed by amino acid sequence alignment and circular dichroism (CD) measurement. We developed a molecular docking model using homology structures of periostin and BMP1/2. Furthermore, we modeled the structural differences among four periostin Fas 1 domains. Greater understanding of how the domains of periostin contribute to BMP1/2 interactions could provide important new information regarding pathological remodeling in the heart and new targets for therapy.

2. Materials and methods

2.1. Cloning, expression, and purification of periostin and BMP1/2

The periostin first Fas1 (97–234) and third Fas1 (368–492) genes were ligated into plasmid pET30a. BMP1 (114–321)/BMP2 (282–396) were subcloned into the N-terminal His-tagged fusion protein vector pET-28a for purification. BMP1/2 was also subcloned into a glutathione S-transferase (GST)-fused protein vector pGEX-4T1 to perform a pull-down assay. The periostin first Fas1 and third Fas1 were transformed into the overexpression host *Escherichia coli* BL21(DE3). A single colony was incubated in 5 ml Luria Betani (LB) medium containing 10 μg/ml of kanamycin at 37 °C overnight. The cell cultures were added to 2 l of LB medium with kanamycin and maintained at 37 °C until the OD_{600} reached 0.5–0.6. Protein expression was induced with 0.5 mM IPTG (isopropyl-thio-β-D-galactopyranoside) for 16 h at 25 °C, after which cells were harvested by centrifugation at 3660*g* for 25 min. The pellets were then resuspended with lysis buffer A [50 mM Tris–HCl (pH 8.0) and 200 mM NaCl] and sonicated on ice. Cell lysates were subsequently centrifuged at 20170*g* for 45 min to remove the supernatant, after which the periostin first Fas1/third Fas1 inclusion bodies were resuspended and sonicated in buffer [50 mM Glycine (pH 10.5)] on ice and centrifuged to remove the supernatant. Following the protein extraction step, samples were loaded onto a Ni-NTA (Amersham-Pharmacia Biotech) column and pre-equilibrated with buffer [50 mM Tris–HCl (pH 10.5) and 200 mM NaCl]. The bound protein was eluted by varying the concentration of imidazole from 20 mM to 200 mM, and the resulting fractions were analyzed by electrophoresis on a 15% SDS–PAGE gel. For the His pull-down assay, glutathione S-transferase (GST)-fused BMP1/2 constructs were transformed into the host *E. coli* BL21(DE3) for expression. Single colonies were then inoculated in 5 ml LB medium enriched with 50 μg/ml ampicillin. Following overnight culture at 37 °C, the cells were added to 2 l of LB medium containing ampicillin. The BMP1/2 cell pellets were then resuspended in lysis buffer (1× PBS) and sonicated on ice. The BMP1/2 pellets were then sonicated in buffer B [50 mM Tris–HCl (pH 8.0), 200 mM NaCl, and 6 M Urea] on ice and the resulting cell lysates were centrifuged. The BMP1/2 supernatants were subsequently loaded onto a glutathione-sepharose column at a flow rate 2.5 ml/min and washed in PBS buffer. The GST-BMP1/2 fusion proteins were then eluted in 5–30 mM glutathione. The GST-BMP1/2 proteins was loaded onto a Q-Sepharose fast-flow (Amersham-Pharmacia Biotech) anion exchange chromatography column pre-equilibrated with buffer A. Finally, the proteins were concentrated by centrifugation at 1320*g* using ultrafiltration devices.

2.2. Western blotting

The purified periostin first Fas1/third Fas1 and BMP1/2 proteins from 15% SDS–PAGE were transferred onto a nitrocellulose membrane at 105 V for 1 h on ice. The membrane was blocked with 5% skim milk in PBS buffer containing 0.1% Tween-20 (PBS-T) for 1 h. After blocking, the membrane was incubated in primary antibody [GST (B-14) diluted 1:2000, and His-probe (G-18) diluted 1:5000, Santa Cruz Biotechnology, Inc.] for 1 h. Following washing with PBS-T for 40 min, the membrane was incubated for 1 h with GST secondary antibody [goat anti-mouse IgG-HRP diluted 1:20000 (Santa Cruz Biotechnology, Inc.)] and His secondary antibody (goat anti-rabbit IgG-HRP diluted 1:100000) in blocking buffer for 1 h.

2.3. Mutagenesis of the periostin first Fas1 and third Fas1

Double-stranded oligonucleotides were used for site-directed mutagenesis of twelve different periostin first Fas1 (K129A, N171A, P186A, N191A, N201A, C208A, and T231A) and third Fas1 residues to alanine (Y444A, Q447A, G454A, Y462A, and R463A).

2.4. Far-ultraviolet circular dichroism spectroscopy analysis

Circular dichroism spectropolarimeter (JASCO J-715) measurements were taken using a 0.1 cm cell at 0.2 nm intervals and 25 °C. The CD (Far-UV circular dichroism) spectra of purified proteins were recorded in the 190–260 nm range. A far-UV CD spectrum was taken at a protein concentration of 0.5 mg/ml. The spectrum was obtained in milli-degrees, and the CD signal was converted to mean residue ellipticity (MRE) prior to secondary-structural analysis. Calculation of the secondary structural elements was performed using the CDNN program.

2.5. His-tagged pull down assay

A total of 50 μg of the purified proteins, periostin first Fas1/third Fas1 and GST-tagged BMP1/BMP2, were mixed with 50 μl Ni-NTA bead in buffer A for 4 h at 4 °C. The supernatants were removed via centrifugation at 805*g* for 3 min and the beads were washed five times with buffer A. Each time, the beads were then incubated with wash buffer on a rotator for 10 min, and then collected by centrifugation. The beads were subsequently eluted with elution buffer [50 mM Tris–HCl (pH 8.0), 200 mM NaCl, and 200 mM Imidazole], boiled in SDS–PAGE sample loading buffer for 5 min, resolved by SDS–PAGE, and visualized by immunoblotting assay using anti-GST and anti-His.

2.6. BIAcore biosensor analysis

Measurements of the apparent dissociation constants (K_D) between periostin and BMP1/2 were performed using a BIAcore 2000 biosensor (Biosensor, Sweden). Periostin first Fas1 and third Fas1 (100 μg/ml in 10 mM sodium acetate with a pH of 4.0) were covalently bound by an amine-coupling method to the carboxylated dextran matrix at a concentration corresponding to 160 RU (response units) according to the manufacturer's protocol. A flow path involving two cells was then employed to simultaneously measure the kinetic parameters from one flow cell containing the periostin first Fas1/third Fas1-immobilized sensor chip to another flow cell containing a blank chip. For kinetic measurements at room temperature, BMP1/2 samples were prepared by dilution with an HBS buffer [150 mM NaCl, 3 mM EDTA, 0.005% surfactant P20, and 10 mM HEPES (pH 4)] ranging in concentrations from 975 nm to 7800 nm. Each sample was injected with 70 μl of BMP1/2 solutions into the flow cells (association phase) at a rate

of 10 μl/min. Among the cycles, the immobilized ligand was regenerated by injecting 30 μl of 50 mM NaOH at 10 μl/min during the cycles.

2.7. Prediction of the secondary and three-dimensional structures

The structural models of periostin and BMP1/2 were constructed using the SWISS-MODEL software. The 3D models of periostin first Fas1 (PDB ID: 1X3B), third Fas1 (PDB ID: 1W7D), BMP1 (PDB ID: 3EDH), and BMP2 (PDB ID: 2H62) were used.

3. Results and discussion

The domain structures of full-length periostin, BMP1, and BMP2 are shown in Fig. 1A. Periostin consists of an EMI domain and four repeated Fas1 domains. BMP1 was divided into metalloproteinase and five CUB domains, while BMP2 was divided into TGF-β polypeptide and TGF-β domains [1,19,20].

While a great deal of progress has been made in research regarding periostin, the 3D structure of periostin has not yet been determined. Interestingly, periostin has four different Fas1

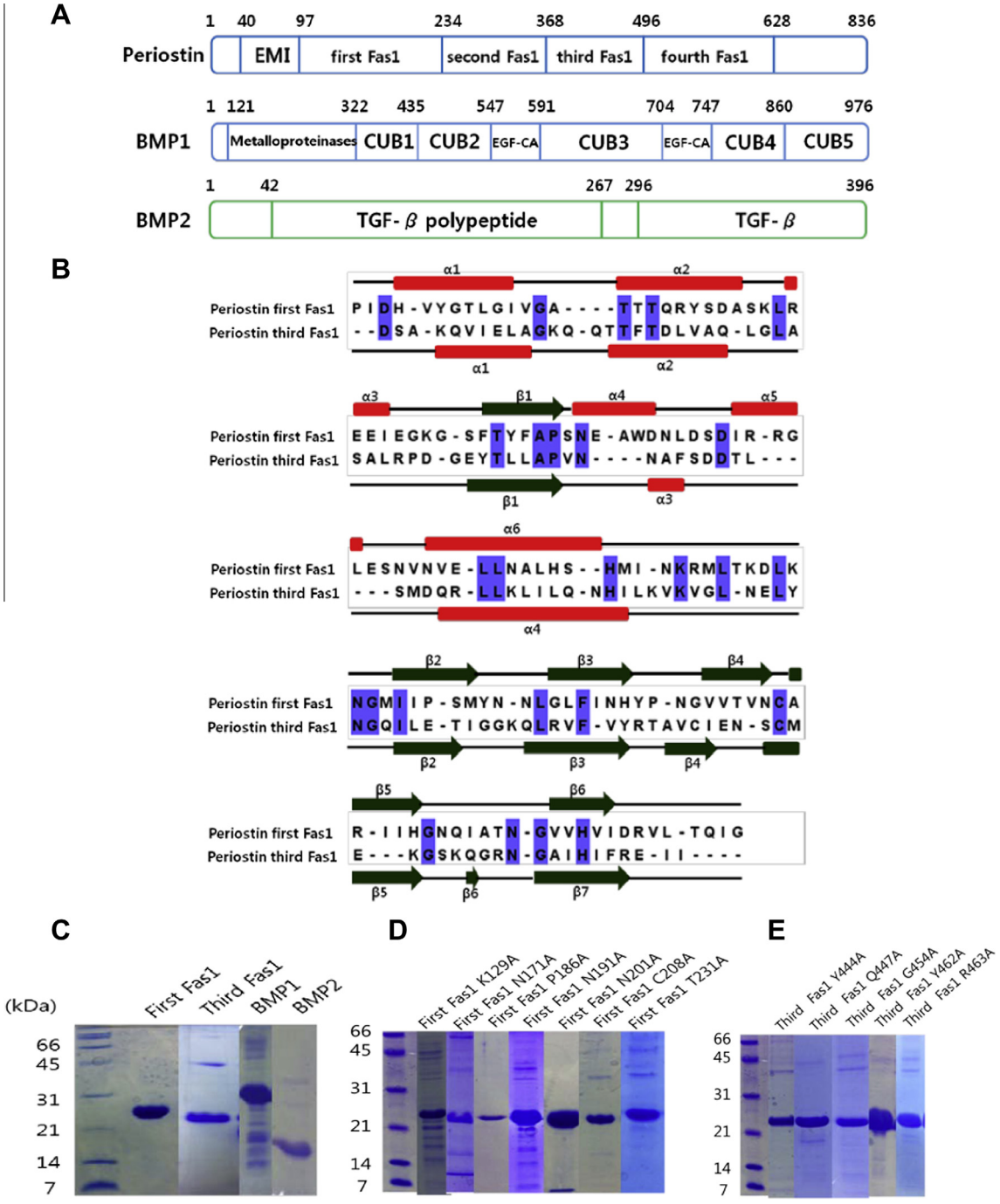

Fig. 1. (A) Schematic diagram showing the domains of the full-length periostin, BMP1, and BMP2. Periostin consists of an EMI domain and four Fas1 domains. BMP1 has a metalloproteinase domain and five CUB domains. BMP2 has a TGF-β polypeptide region and a TGF-β region. (B) Predicted secondary structures and sequence alignments of periostin first Fas1 and third Fas1. The conserved amino acids of the periostin first Fas1 and third Fas1 domains are shown in blue color boxes. α-Helices are represented as red ellipses and β-sheets as green arrows. (C–E) Purification of periostin first Fas1, third Fas1, BMP1 (114–321), BMP2 (282–396), and their mutations. (For interpretation of the references to color in this figure legend, the reader is referred to the web version of this article.)

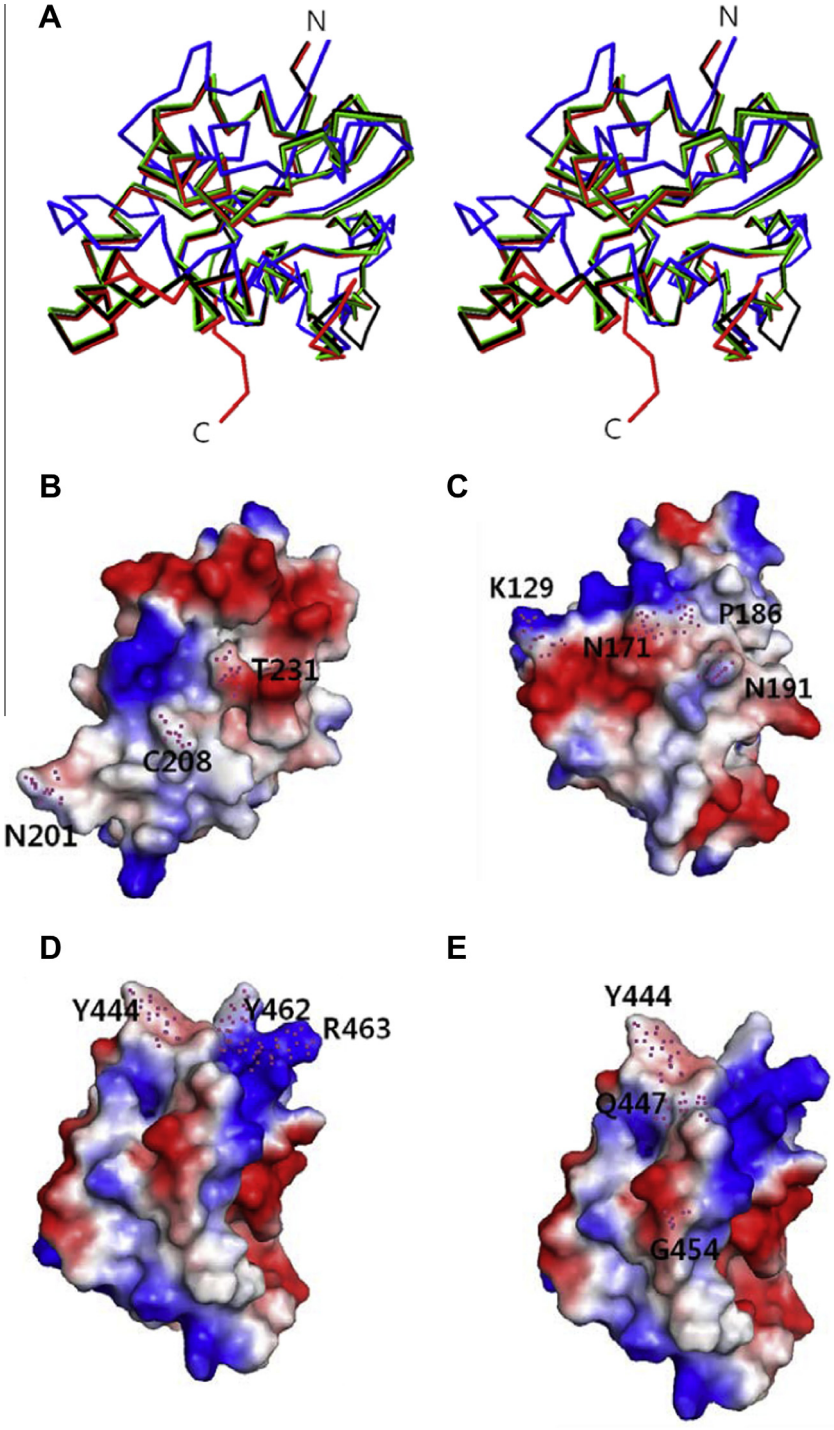

Fig. 2. (A) Superposition of Cα traces of four modeled periostin Fas1 domains. The protein is shown in red for the first Fas1, green for the second Fas1, blue for the third Fas1 and black for the fourth Fas1. (B–E) The 3D modeled structures of the first Fas1 and the third Fas1 of periostin are shown as surface representations. Blue and red represent positive and negative electrostatic potentials, respectively. The binding sites between first Fas1/third Fas1 of periostin and BMP1/BMP2 are also illustrated. (For interpretation of the references to color in this figure legend, the reader is referred to the web version of this article.)

domains. The sequence similarities among these domains are very low, and they only include about 10 conserved amino acids (Fig. S1). Despite very low sequence homologies among the Fas1 domains in periostin, we found that the predicted structure was unexpectedly similar to those of the second and fourth Fas 1 domains. To investigate the differences between the first Fas1 and third Fas1 domains, the secondary structures of periostin first Fas1 and third Fas1 were predicted. Periostin first Fas1 has six α-helices and six β-sheets, while periostin third Fas1 has four α-helices and seven β-sheets, as shown in Fig. 1B. The sequence of periostin first Fas1 was only slightly similar to that of third Fas1, with 18% identity. All purified wild-type and mutation proteins were visualized by SDS–PAGE and Coomassie blue staining, as shown in Fig. 1C–E. His-tagged periostin first Fas1 and third Fas1 showed identical positions at 25 kDa and 23 kDa, respectively. The concentrations of periostin first Fas1 mutants (K129A, N171A,

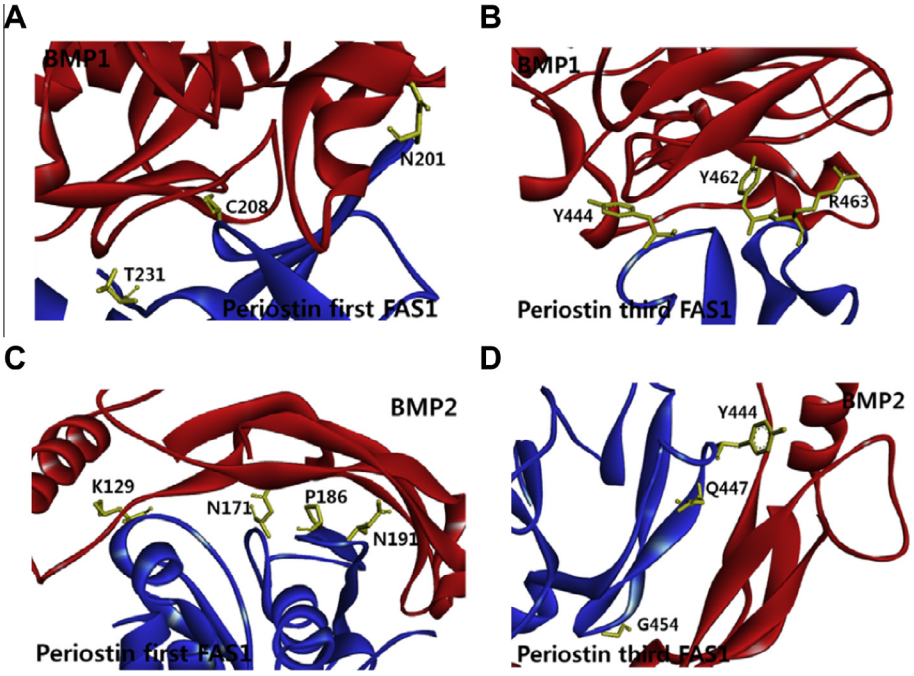

Fig. 3. The models of the periostin first Fas1/third Fas1 (blue) and BMP1/BMP2 (red) complex structures are shown as ribbon representations. (A and B) Predictions of the binding sites (N201, C208, and T231) between periostin first Fas 1 and BMP1 and those (Y444, Y462, and R463) between periostin third Fas 1 and BMP1 are shown in green. (C and D) Predictions of the binding sites (K129, N171, P186, and N191) between periostin first Fas1 and BMP2 and those (Y444, Q447, and G454) between periostin third Fas1 and BMP2 are shown in green. (For interpretation of the references to color in this figure legend, the reader is referred to the web version of this article.)

P186A, N191A, N201A, C208A, and T231A), third Fas1 mutants (Y444A, Q447A, G454A, Y462A, and R463A), BMP1 (114–321), and BMP2 (282–396) showed positions at 25 kDa, 23 kDa, 30 kDa, and 16 kDa, respectively.

The full-length (1–836) of periostin exhibits approximately 43% sequence similarity with the full-length (1–683) of human transforming growth factor-beta induced protein ig-h3 (TGFBIp, ßig-h3). We found that the structures of the first, second, and fourth Fas1 domains in periostin were similar to those of the fourth Fas 1 domain of TGFBIp from the modeled 3D structures, with 27, 27, and 34% homology, respectively. The three-dimensional NMR structure (PDB ID: 1X3B) of the fourth Fas 1 domain of human TGFBIp has previously been elucidated [21]. The structure of the third Fas 1 domain in periostin is different from those of the first, second, and fourth Fas1 domains, and we found that it is similar to the NMR structure of Fasciclin-like protein from *Rhodobacter sphaeroides* (PDB ID: 1w7d) with 23% sequence identity [22]. Structural comparison between the Fas 1 domain and TGFBIp or fasciclin domain of Fasciclin-like protein may improve our understanding of the biological function of the unknown Fas 1 domain. FAS1 domains play important roles in cell adhesion, which are not understood, despite many structural and functional studies. TGFBIp (βig-h3) and periostin are FAS1 domain proteins that function in angiogenesis and development of cornea and bone, and are also highly expressed in cancer tissues [21]. The root mean squared deviations (r.m.s.d.) (Cα) of first–second, first–fourth, and second–fourth Fas 1 domains in periostin determined by PyMOL were reliable low values of 0.121 Å, 0.485 Å, and 0.059 Å, respectively, while those of the first–third, second–third, and third–fourth Fas 1 domains, including the third domain of periostin, were very high, being 4.439 Å, 2.627 Å, and 3.297 Å, respectively (Fig. 2A). Based on these results, the structural and functional roles of periostin third Fas 1 will be very different from those of the first, second, and fourth Fas 1 domains. The 3D modeled structures of the first Fas1 and the third Fas1 of periostin are shown as surface representations (Fig. 2B–E). The binding sites between first Fas1/third Fas1 of periostin and BMP1/BMP2 are also illustrated and used to implement point mutations on the complex surface.

Models of the three-dimensional structures of periostin first Fas1/third Fas1 were generated. The structures of periostin first Fas1 (PDB ID: 1X3B, 98–234), third Fas1 (PDB ID: 1W7D, 370–492), BMP1 (PDB ID: 3EDH, 121–321), and BMP2 (PDB ID: 2H62, 293–396) were identified. The results of interactions between periostin first Fas1/third Fas1 and BMP1/2 were observed (Fig. 3). We predicted the interaction sites using the modeled complex structures. Six or seven residues of periostin were selected for mutation to investigate the interaction between periostin and BMP1/BMP2. The periostin-BMP1 interactions were localized at the residues of periostin first Fas1 (N201, C208, and T231) and periostin third Fas1 (Y444, Y462, and R463). The periostin-BMP2 interactions were localized at the residues of periostin first Fas1 (K129, N171, P186, and N191) and periostin third Fas1 (Y444, Q447, and G454). Interestingly, the Y444 residue of periostin was assumed to play an important role in binding with both BMP1/BMP2.

The circular dichroism (CD) spectra of purified periostin first Fas1/third Fas1 or BMP1/BMP2 exhibited two negative maxima (Fig. S2A and B). We found that the periostin third Fas1 or BMP2 spectra produced more negative peaks than those of periostin first Fas1 or BMP1 with loss of the secondary structure (α-helix and β-sheet elements). The spectrum of the wild-type periostin first Fas1 was similar to that of the mutant C208A and T231A, but quite different from that of the mutant N201A (Fig. S2C). The N201A curve produced the greatest negative peak, whereas the curves of C208A and T231A were less negative. The wild-type periostin first Fas1 was similar to the mutants K129A, N171A, P186A, and N191A (Fig. S2D). Likewise, the spectrum of the wild-type periostin third Fas1 was similar to those of the mutants Y444A, Q447A, and G454A, but quite different from those of the mutants Y462A and R463A. The Y462 and R463A curves produced the greatest negative peaks, whereas the curve of Y444A was less negative (Fig. S2E and F). The CD spectra of the periostin mutants showed that each

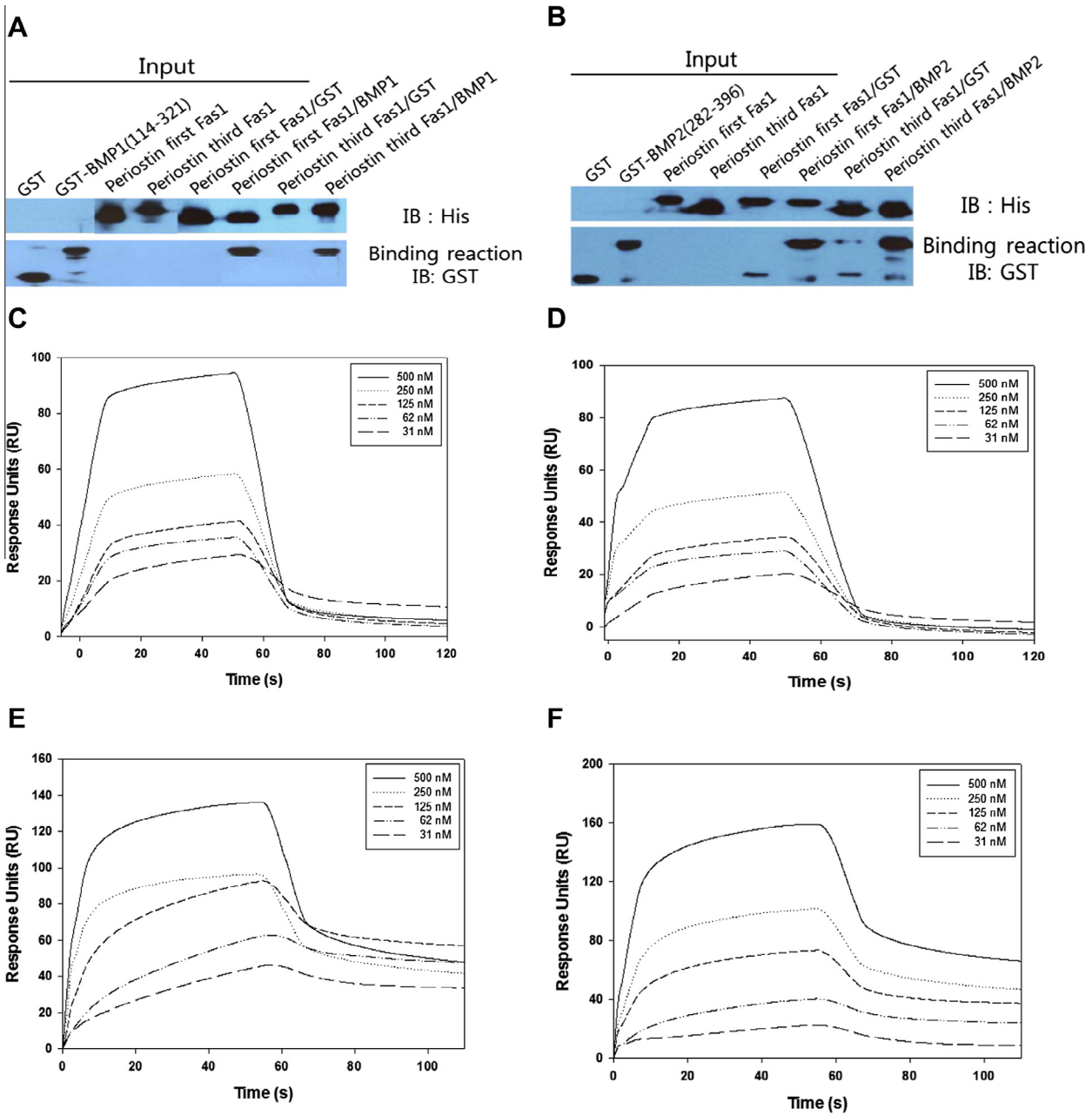

Fig. 4. (A and B) Interaction analyses of periostin first Fas1/third Fas1 and BMP1/2. Analysis of periostin and GST-BMP1/BMP2 using His-tag pull down assay *in vitro*. (C and D) BIAcore biosensor analysis of the binding of periostin first Fas1/third Fas1 to BMP1. The sensorgrams for 31, 62, 125, 250, and 500 nM are shown. (E and F) BIAcore biosensor analyses showed that periostin first Fas1/third Fas1 bound to BMP2. Periostin first Fas1/third Fas1 was immobilized to the dextran matrix, after which different concentrations of BMP1/BMP2 were injected.

mutation affected the conformation of periostin to a different extent. The structural changes induced by three mutants (N201A, Y462A, and R463A) were more significant than those induced by the wild type.

GST-BMP1 (121–321) and GST-BMP2 (293–396) fusion proteins were used in the pull down of His-tagged periostin first Fas1/third Fas1. As a result, the periostin first Fas1/third Fas1 residues interacted with BMP1/BMP2 (Fig. 4A and B). The binding affinities of periostin and BMP1/BMP2 were estimated by surface plasmon resonance spectroscopy (BIAcore 2000) (Fig. 4C–F). Sensorgrams of periostin first Fas1/third Fas1 binding to BMP1/2 were used to calculate kinetic binding constants. The background sensorgrams were then subtracted from the experimental sensorgrams, yielding representative specific binding constants. We found that periostin first Fas1 and third Fas1 physically bound to BMP1 with apparent K_D (dissociation constants) values of 37 nM and 24 nM, respectively. In addition, periostin first Fas1 and third Fas1 physically bound to BMP2 with apparent K_D values of 18 nM and 15 nM, respectively. As a result, periostin first Fas1 and third Fas1 more strongly bound to BMP1 than BMP2. Based on these results, we modeled the secondary and three-dimensional structures of periostin and BMP1/2 complexes and illustrated the interaction and specific binding sites of periostin and BMP1/2 *in vitro*. We found that the structures of the first, second, and fourth Fas1 domains in periostin were similar to that of the fourth Fas 1 domain of TGFBIp. The structure of the third Fas 1 domain in periostin was different from those of the first, second, and fourth Fas1 domains, but similar to the NMR structure of Fasciclin-like protein from

R. sphaeroides. These results will useful in future analyses of the biological action and function of the interaction between periostin and bone morphogenetic protein.

Acknowledgments

This study was supported by the Basic Science Research Program through the National Research Foundation of Korea (NRF) funded by the Ministry of Education, Science and Technology (2013-054737) to S.B.J and (2013-054754) M.S.J.

Appendix A. Supplementary data

Supplementary data associated with this article can be found, in the online version, at http://dx.doi.org/10.1016/j.bbrc.2014.05.055.

References

[1] K. Horiuchi, N. Amizuka, S. Takeshita, H. Takamatsu, M. Katsuura, H. Ozawa, Y. Toyama, L.F. Bonewald, A. Kudo, Identification and characterization of a navel protein periostin, with restricted expression to periosteum and periodontal ligament and increased expression by transforming growth factor β, J. Bone Miner. Res. 14 (1999) 1239–1249.
[2] D. Wang, S. Oparil, J.A. Feng, P. Li, G. Perry, L.B. Chen, M. Dai, S.W. John, Y.F. Chen, Effects of pressure overload on extracellular matrix expression in the heart of the atrial natriuretic peptide-null mouse, Hypertension 42 (2003) 88–95.
[3] R.A. Norris, B. Damon, V. Mironov, V. Kasyanov, A. Ramamurthi, R. Moreno-Rodriguez, T. Trusk, J.D. Potts, R.L. Goodwin, J. Davis, S. Hoffman, X. Wen, Y. Sugi, C.B. Kern, C.H. Mjaatvedt, D.K. Turner, T. Oka, S.J. Conway, J.D. Molkentin, G. Forgacs, R.R. Markwald, Periostin regulates collagen fibrillogenesis and the biomechanical properties of connective tissues, J. Cell. Biochem. 101 (2007) 695–711.
[4] S. Takeshita, R. Kikuno, K. Tezuka, E. Amann, Osteoblast-specific factor 2: cloning of a putative bone adhesion protein with homology with the insect protein fasciclin I, Biochem. J. 294 (1993) 271–278.
[5] J. Litvin, S. Zhu, R. Norris, R. Markwald, Periostin family of proteins: therapeutic targets for heart disease, Anat. Rec. A Discov. Mol. Cell. Evol. Biol. 287 (2005) 1205–1212.
[6] J.T. Butcher, R.A. Norris, S. Hoffman, C.H. Mjaatvedt, R.R. Markwald, Periostin promotes atrioventricular mesenchyme matrix invasion and remodeling mediated by integrin signaling through Rho/PI 3-kinase, Dev. Biol. 302 (2007) 256–266.
[7] A. Kruzynska-Frejtag, M. Machnicki, R. Rogers, R.R. Markwald, S.J. Conway, Periostin (an osteoblast-specific factor) is expressed within the embryonic mouse heart during valve formation, Mech. Dev. 103 (2001) 183–188.
[8] V. Lindner, Q. Wang, B.A. Conley, R.E. Friesel, C.P. Vary, Vascular injury induces expression of periostin: implications for vascular cell differentiation and migration, Arterioscler. Thromb. Vasc. Biol. 25 (2005) 77–83.
[9] P. Li, S. Oparil, W. Feng, Y.F. Chen, Hypoxia-responsive growth factors upregulate periostin and osteopontin expression via distinct signaling pathways in rat pulmonary arterial smooth muscle cells, J. Appl. Physiol. 97 (2004) 1550–1558.
[10] M. Shimazaki, A. Kudo, Impaired capsule formation of tumors in periostin-null mice, Biochem. Biophys. Res. Commun. 367 (2008) 736–742.
[11] Y. Kudo, I. Ogawa, S. Kitajima, M. Kitagawa, H. Kawai, P.M. Gaffney, M. Miyauchi, T. Takata, Periostin promotes invasion and anchorage-independent growth in the metastatic process of head and neck cancer, Cancer Res. 66 (2006) 6928–6935.
[12] H. Sasaki, K.M. Lo, L.B. Chen, D. Auclair, Y. Nakashima, S. Moriyama, I. Fukai, C. Tarn, M. Loda, Y. Fujii, Expression of periostin, homologous with an insect cell adhesion molecule, as a prognostic marker in non-small cell lung cancers, Jpn. J. Cancer Res. 92 (2001) 869–873.
[13] Y. Zhang, G. Zhang, J. Li, Q. Tao, W. Tang, The expression analysis of periostin in human breast cancer, J. Surg. Res. 160 (2010) 102–106.
[14] T. Maruhashi, I. Kii, M. Saito, A. Kudo, Interaction between periostin and BMP-1 promotes proteolytic activation of lysyl oxidase, J. Biol. Chem. 285 (2010) 13294–13303.
[15] N. Hartigan, L. Garrigue-Antar, K.E. Kadler, Bone morphogenetic protein-1 (BMP-1) Identification of the minimal domain structure for procollagen c-proteinase activity, J. Biol. Chem. 278 (2003) 18045–18049.
[16] X. Ji, D. Chen, C. Xu, S.E. Harris, G.R. Mundy, T. Yoneda, Patterns of gene expression associated with BMP-2-induced osteoblast and adipocyte differentiation of mesenchymal progenitor cell 3T3-F442A, J. Bone Miner. Metab. 18 (2000) 132–139.
[17] L. Grgurevic, B. Macek, M. Mercep, M. Jelic, T. Smoljanovic, I. Erjavec, I. Dumic-Cule, S. Prgomet, D. Durdevic, D. Vnuk, M. Lipar, M. Stejskal, V. Kufner, J. Brkljacic, D. Maticic, S. Vukicevic, Bone morphogenetic protein (BMP)1–3 enhances bone repair, Biochem. Biophys. Res. Commun. 408 (2011) 25–31.
[18] R. Ruppert, E. Hoffmann, W. Sebald, Human bone morphogenetic protein 2 contains a heparin-binding site which modifies its biological activity, Eur. J. Biochem. 237 (1996) 295–302.
[19] K. Inai, R.A. Norris, S. Hoffman, R.R. Markwald, Y. Sugi, BMP-2 induces cell migration and periostin expression during atrioventricular valvulogenesis, Dev. Biol. 315 (2008) 383–396.
[20] Y.J. Lee, I.S. Kim, S.A. Park, Y. Kim, J.E. Lee, D.Y. Noh, K.T. Kim, S.H. Ryu, P.G. Suh, Periostin-binding DNA aptamer inhibits breast cancer growth and metastasis, Mol. Ther. 21 (2013) 1004–1013.
[21] M. Yoneyama, T. Tomizawa, N. Tochio, S. Koshiba, M. Inoue, T. Kigawa, S. Yokoyama, Solution structure of the FAS1 domain of human transforming growth factor-beta induced protein IG-H3 (in press).
[22] R.G. Moody, M.P. Williamson, Structure and function of a bacterial fasciclin I domain protein elucidates function of related cell adhesion proteins such as TGFBIp and periostin, FEBS Open Bio 3 (2013) 71–77.